Journal of Biomolecular NMR, 8 (1996) 319–330
ESCOM

J-Bio NMR 379

Doubly sensitivity-enhanced 3D TOCSY-HSQC

Sybren S. Wijmenga[a,*], Carlo P.M. van Mierlo[b] and Elles Steensma[b]

[a]*Nijmegen SON Research Center for Molecular Design, Structure and Synthesis, SON/NWO National HF-NMR Facility, Toernooiveld, 6525 ED Nijmegen, The Netherlands*
[b]*Department of Biochemistry, Wageningen Agricultural University, Dreyenlaan 3, 6703 HA Wageningen, The Netherlands*

Received 9 April 1996
Accepted 3 July 1996

Keywords: B_0 gradients; INEPT; COS-INEPT; Multidimensional NMR; Sensitivity enhancement; TOCSY-HSQC; HSQC; Flavodoxin

Summary

Recently, strategies for double sensitivity enhancement in heteronuclear three-dimensional NMR experiments were introduced (Krishnamurthy, V.V. (1995) *J. Magn. Reson.*, **B106**, 170–177; Sattler et al. (1995) *J. Biomol. NMR*, **6**, 11–22; Sattler et al. (1995) *J. Magn. Reson.*, **B108**, 235–242). Since a sensitivity enhancement of a factor $2^{1/2}$ can be achieved for each indirect dimension, nD spectra can theoretically be enhanced up to a factor of $2^{((n-1)/2)}$. We propose and analyze a doubly enhanced three-dimensional TOCSY-HSQC sequence. The application of the doubly enhanced three-dimensional {^{15}N,^{1}H} TOCSY-HSQC sequence is shown for uniformly ^{13}C-/^{15}N- and ^{15}N-labeled samples of the relatively large *Azotobacter vinelandii* flavodoxin II (179 amino acids). The main factors that contribute to the final signal-to-noise enhancement have been systematically investigated. The sensitivity enhancement obtained for the doubly enhanced TOCSY-HSQC pulse sequence as compared to the standard (unenhanced) version is close to the theoretically expected factor of two.

Introduction

Pulse sequences employing B_0 field gradients have been shown to yield spectra of very high quality with respect to artifact and solvent suppression (Jahnke and Kessler, 1994; Schleucher et al., 1994; Stonehouse et al., 1994, 1995; Kontaxis et al., 1994; Kay, 1995; Sattler et al., 1995a,b). B_0 field gradients can eliminate the undesired signals in NMR spectra in at least two distinct ways. In the first approach, signals resulting from unwanted coherence pathways are rejected. The gradients are applied each time the signal of interest lies along the z-axis so that (hopefully) all unwanted coherences are defocussed. This approach thus provides an additional means over phase cycling for removing artifacts, with the advantage that artifacts can be removed per individual scan (Bax and Pochapsky, 1992; Keeler et al., 1994). Even better artifact and solvent suppression is obtained in the second approach, in which the gradients are used to actively select coherence pathways of interest (Jahnke and Kessler, 1994; Kay, 1995; Sattler et al., 1995a,b).

Initially, it was thought that the use of gradients to actively select coherence pathways would lead to a loss in sensitivity by a factor of $2^{1/2}$ as compared to the conventional phase-cycled experiments, since only one of the two possible coherence pathways is selected. Therefore, the first approach, in which unwanted coherence pathways are rejected and which thus has the same sensitivity as a phase-cycled experiment, was favored (e.g. Bax and Pochapsky, 1992; Keeler et al., 1994). Later, Kay et al. (1992) demonstrated that instead of a lower sensitivity, in fact an enhanced sensitivity can be achieved via the second approach when used in combination with the enhanced INEPT sequence (eINEPT) developed by Rance et al. (Cavanagh and Rance, 1990; Palmer III et al., 1991). The eINEPT sequence gives a factor of $2^{1/2}$ higher sensitivity as compared to the regular INEPT sequence, since it allows to retain both coherence pathways. Because the gradients also select these two coherence pathways, no signal loss is incurred. Subsequently, the corresponding theoretical background was thoroughly analyzed by Keeler and co-workers (Keeler et al., 1994; Kontaxis et al., 1994; Stonehouse et al., 1994,1995) and by Griesinger et al. (Schleucher et al., 1994). Sequences such as

*To whom correspondence should be addressed at: Department of Biochemistry and Biophysics, Umeå University, S-901 87 Umeå, Sweden.

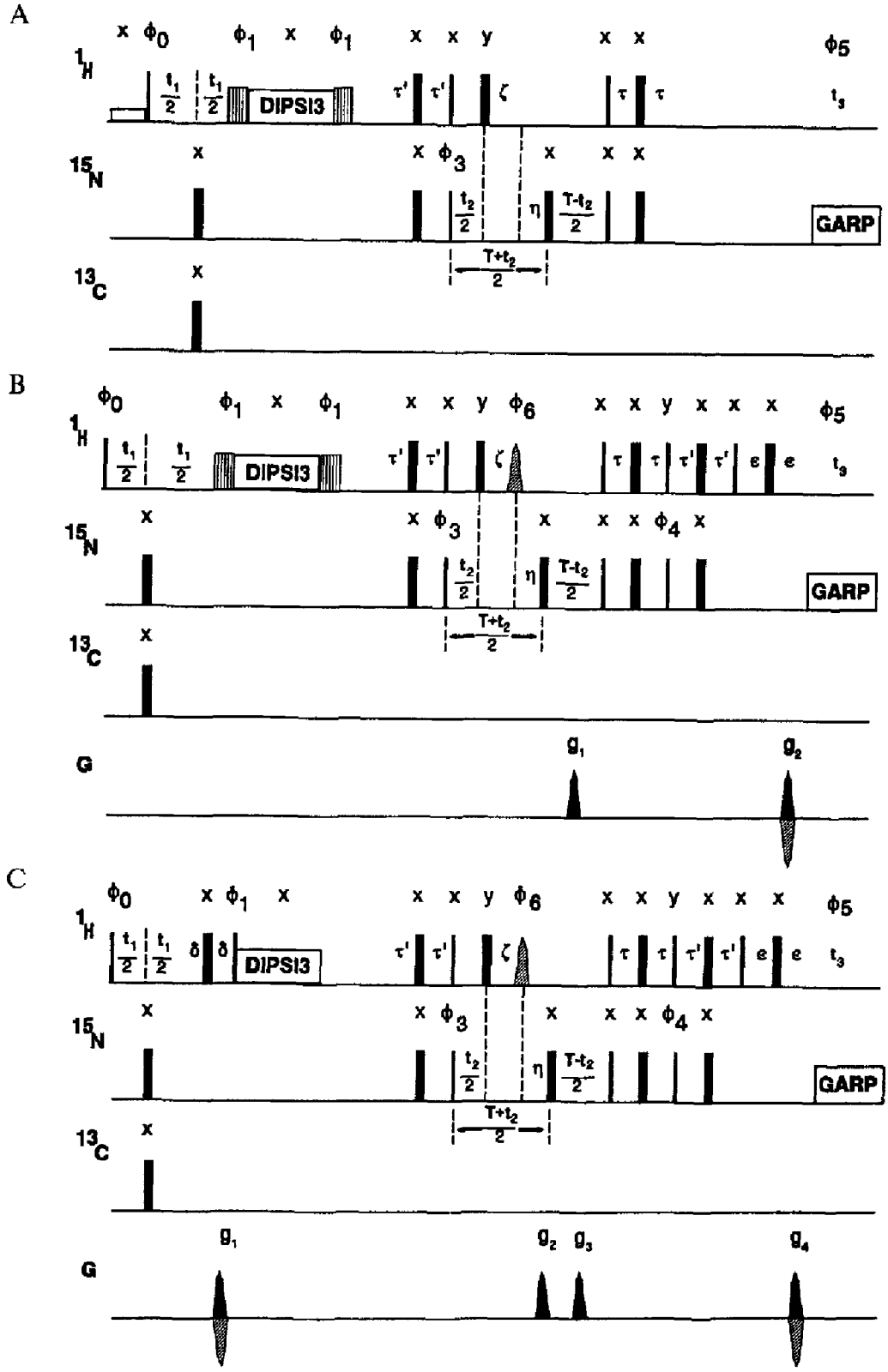

Fig. 1. Pulse sequences used for 3D TOCSY-HSQC experiments. Narrow bars indicate rf pulses with a 90° flip angle, while wider bars indicate rf pulses with a 180° flip angle. The 90° water flip-back pulse has a Gaussian profile and a duration of 2.1 ms. All B_0 field gradients are sine-bell shaped. The 1 ms trim pulses bracketing the DIPSI3 sequence are indicated by vertical lines. (A) Standard 3D TOCSY-HSQC pulse sequence. The phase cycle used is: $\phi_0 = y,y,-y,-y$; $\phi_1 = x$; $\phi_3 = x,-x$; $\phi_5 = x,-x,-x,x$. Quadrature detection in the t_1 and the t_2 dimension is obtained by using the STATES-TPPI method (Marion et al., 1989) in which the phases ϕ_0 and ϕ_3 are incremented separately. (B) Singly sensitivity-enhanced 3D TOCSY-HSQC pulse sequence. The phase cycle used is: $\phi_0 = y,y,-y,-y$; $\phi_1 = x$; $\phi_3 = x,-x$; $\phi_4 = y$; $\phi_5 = x,-x,-x,x$. Optimal sensitivity for rapidly exchanging amide

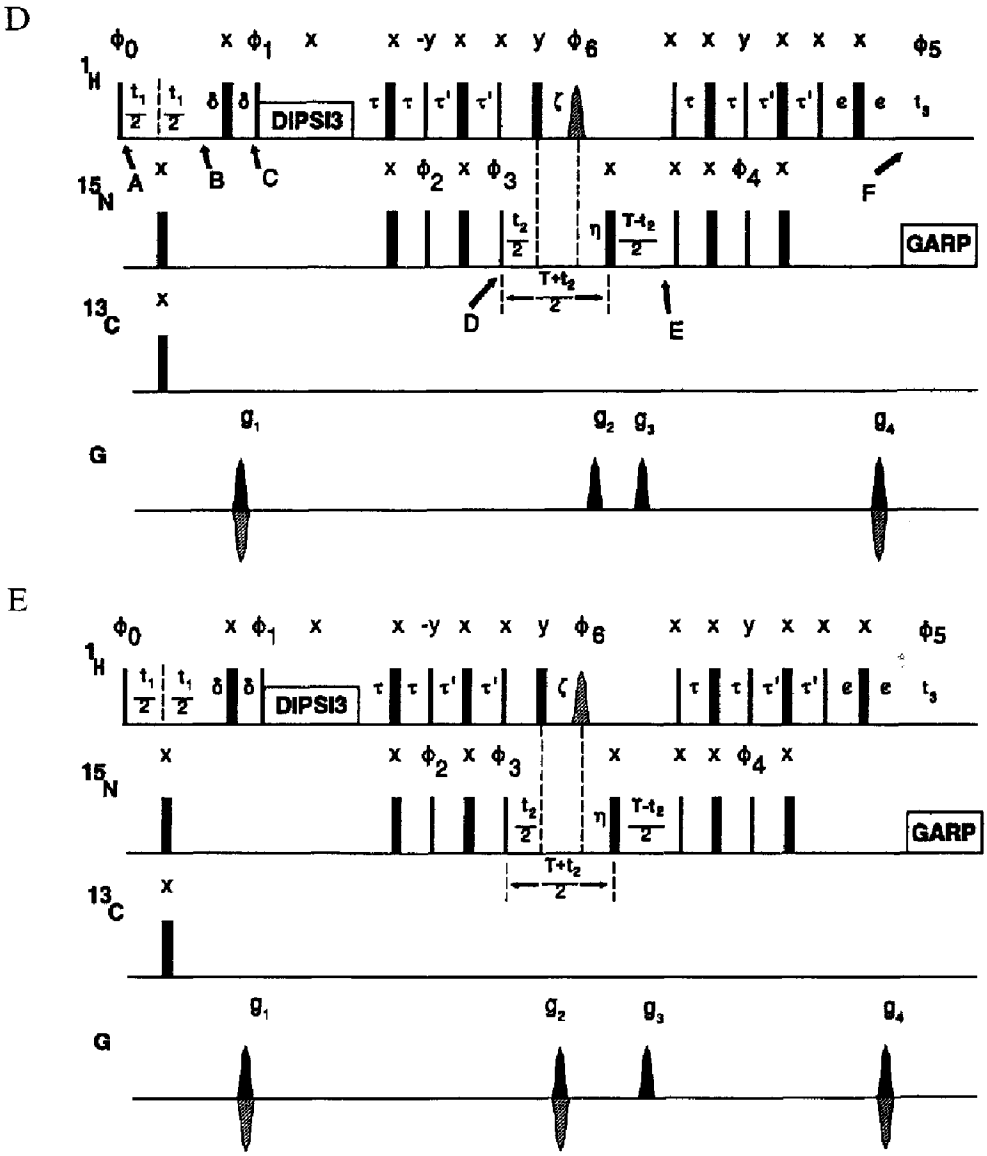

protons is achieved when $\phi_6 = y$, as the water magnetization is not defocussed by the gradients and lies along the +z-axis just prior to acquisition. Quadrature detection in the t_1 dimension is obtained via the STATES-TPPI method by incrementing phase ϕ_0. Absorption-mode spectra in the t_2 dimension are obtained by separate measurements of the N- and P-type coherences, which is achieved by simultaneously inverting the sign of the final gradient and of phase ϕ_4, as described in the text. The amplitudes and durations of gradients 1 and 2 are equal to those of the third and fourth gradients of sequence 1D. (C) Singly sensitivity-enhanced 3D TOCSY-HSQC pulse sequence with coherence pathway selection by gradients on going from t_1 to t_2. The phase cycle used is: $\phi_0 = y$; $\phi_1 = x$; $\phi_3 = x,-x$; $\phi_4 = y$; $\phi_5 = x,-x$; $\phi_6 = y$. Water magnetization is dephased for any setting of ϕ_6 (see text). Absorption-mode spectra in the t_1 dimension are obtained by separate measurements of N-type and P-type coherences, by inverting the sign of the first gradient as described in the text; absorption-mode spectra in the t_2 dimension are obtained as discussed for sequence 1B. Gradient amplitudes and durations used are the same as for sequence 1D. (D) Doubly sensitivity-enhanced 3D TOCSY-HSQC pulse sequence. The phase cycle used is: $\phi_0 = y$; $\phi_1 = x$; $\phi_2 = x,-x$; $\phi_3 = y,-y$; $\phi_4 = y$; $\phi_5 = x,-x$; $\phi_6 = -x$. Water magnetization is dephased for any setting of ϕ_6 (see text). Absorption-mode spectra in the t_1 dimension are obtained by separate measurements of N- and P-type coherences, which is done by inverting the sign of the first gradient in concert with the sign of phase ϕ_1, as described in the text; absorption-mode spectra in the t_2 dimension are obtained as described for sequence 1B. For gradients 1 to 4 the amplitudes used are 16, 40, 80 and 16, respectively (with 100 corresponding to 60 G/cm) and the corresponding durations are 0.125, 0.5, 0.5 and 0.25 ms, respectively. (E) Doubly sensitivity-enhanced 3D TOCSY-HSQC pulse sequence, optimized for maximal sensitivity of rapidly exchanging amide protons; the water magnetization is not defocussed and lies along the +z-axis just prior to acquisition. The phases used are identical to those in sequence 1D, except for ϕ_6, which is set to x. Absorption-mode spectra in both the t_1 and the t_2 dimension are obtained as described for sequence 1D, with the exception that in order to refocus the water magnetization $|g_2|\tau_2 = |g_1|\tau_1$ with $s1 = -s2$, and coherence pathway selection in the t_1 and the t_2 dimension is obtained by proper setting of the other gradient amplitudes and signs, as described in the text (gradient strengths used are 24.5, 13.1, 83.2 or 76.8, and 20.4 for gradients 1 to 4, respectively). The INEPT delays τ and τ' are set to 2.3 ms. The length of the constant-time period T is 9 ms, and $\zeta + \eta = T/2$. The delays δ and ε are set to 0.25 and 0.5 ms, respectively, which includes both the gradient length and the recovery time. Nitrogen decoupling during acquisition is achieved via a GARP sequence (Shaka et al., 1985) with a 2 kHz rf field. A 46.6 ms DIPSI3 sequence of 8.7 kHz (Shaka et al., 1988) is used for $^1H,^1H$ TOCSY transfer. The ^1H, ^{15}N and ^{13}C carrier positions are at the H_2O resonance frequency, 110 ppm and 47 ppm, respectively. The ^1H, ^{15}N and ^{13}C pulses are applied with rf field strengths corresponding with 90° pulse lengths of 13, 24 and 20 μs, respectively.

the enhanced INEPT were termed coherence order selective coherence transfer (COS-CT) by Griesinger et al., since such sequences transfer the coherence order completely, e.g. $2I_zS^+ \rightarrow I^+$. Regular INEPT sequences, on the other hand, mix the coherence orders on transfer, e.g. $2I_zS^+ \rightarrow I^+ + I^-$. The coherence transfer sequences that transfer in-phase coherence, e.g. $S^+ \rightarrow I^+$, require an additional J-refocussing period and were termed ICOS-CT. It was also shown that the heteronuclear cross-polarization sequence can be modified into a COS-CT (eCP), and that by adding an additional J-coupling refocussing period it can be modified into an ICOS-CT (Schleucher et al., 1994; Sattler et al., 1995a,b).

In nD NMR experiments employing COS-CT or ICOS-CT sequences instead of regular CT sequences, an improvement by a factor of $2^{((n-1)/2)}$ in sensitivity can be achieved as compared to non-enhanced experiments. Krishnamurthy (1995) was probably the first to demonstrate double enhancement in a 3D NMR experiment (HSQC-TOCSY); however, without using gradients for coherence pathway selection. The caveat of the use of such singly, doubly or multiply enhanced approaches is that apart from a gain in signal intensity also a loss of signal intensity may occur. This is mainly due to four effects:

(1) A larger number of pulses is required in eINEPT as well as in eCP pulse sequences, which leads to signal loss due to rf inhomogeneity.

(2) The eINEPT and eCP pulse sequences are longer than their unenhanced counterparts. This leads to signal loss due to transverse relaxation.

(3) Sattler et al. (1995a,b) showed that the delays required for optimal enhancement in eINEPT sequences depend on the XHn multiplicity. The eINEPT sequence cannot be simultaneously optimized for all multiplicities. Similarly, for eCP sequences the mixing time cannot be optimized for all multiplicities simultaneously.

(4) Application of gradients for coherence pathway selection requires initial defocussing followed by a refocussing of the wanted coherences. The latter is achieved after a waiting period, so that the refocussing may be incomplete due to translational diffusion of the sample molecules during this period.

Interestingly, the original application of enhancement, which is in the context of homonuclear TOCSY, does not require a significantly longer pulse sequence (Cavanagh and Rance, 1990) and does not suffer from these detrimental effects.

To successfully modify existing sequences into enhanced versions, it is required that such sequences contain as COS-CT steps either homonuclear TOCSYs, or $S \rightarrow I$ coherence transfer steps that are short enough to fulfil the condition $2^{1/2} * \exp -\tau/T2 > 1$, with $\tau = 1/(2J_{SI})$ and T2 the transverse relaxation time. In 3D HCCH experiments, double enhancement is therefore expected to give signal-to-noise improvements because of the large $^1J_{CH}$ couplings present and the use of a homonuclear transfer step (Schleucher et al., 1994; Sattler et al., 1995a,b). However, a sensitivity loss may be incurred due to multiplicity effects. Sattler et al. (1995a,b) demonstrated the implementation of the double enhancement procedure in a 3D HCCH experiment using refocussed eINEPTs as COS-CT steps. The doubly enhanced 3D HCCH experiment contains short $C \rightarrow H$ and $C \rightarrow C$ transfer steps and indeed gave an additional enhancement as compared to the singly enhanced 3D HCCH experiment, depending on the multiplicity involved. On the other hand, most 3D triple resonance experiments contain $C \rightarrow N$ or $C \rightarrow P$ transfer steps involving relatively small J-couplings. As a consequence, the durations in such doubly enhanced sequences will take too much time, particularly for large proteins or nucleic acids. It was indeed observed that the doubly enhanced 3D HNCO experiment, which contains a long $C \rightarrow N$ transfer period, did not have an improved sensitivity with respect to the singly enhanced 3D HNCO experiment (Sattler et al., 1995a).

The 3D {^{15}N,^{1}H} TOCSY-HSQC experiment is ideally suited for obtaining sensitivity improvement via the double enhancement approach, since it features (i) a homonuclear $^1H \rightarrow {}^1H$ TOCSY transfer step; (ii) a $^1H \rightarrow {}^{15}N$ INEPT step as well as a $^{15}N \rightarrow {}^1H$ reverse INEPT step, both of which require only approximately 5 ms; and because (iii) multiplicity effects do not play a role. In this paper, we present the implementation of the double enhancement approach in a 3D TOCSY-HSQC experiment. The main factors contributing to the signal-to-noise enhancement are systematically investigated; uniformly ^{13}C-/^{15}N- and ^{15}N-labeled H_2O samples of flavodoxin II of *Azotobacter vinelandii* (179 amino acid residues, 20 kDa) are used for this purpose. It is demonstrated that the sensitivity can be improved by nearly a factor of 2.

Analysis of 3D TOCSY-HSQC sequences

Figure 1 shows the pulse sequences for different versions of the 3D TOCSY-HSQC experiment. The standard non-enhanced version of the experiment is given in Fig. 1A. In the singly enhanced versions only the second transfer step is enhanced, either without (Fig. 1B) or with (Fig. 1C) coherence pathway selection by gradients during the first transfer step. The doubly enhanced version is presented in Fig. 1D. In the standard 3D TOCSY-HSQC experiment (Fig. 1A) the coherence transfer from ^{1}H to ^{15}N takes place via a homonuclear {^{1}H,^{1}H} TOCSY and a subsequent INEPT sequence. In the doubly enhanced version of the 3D TOCSY-HSQC experiment (Fig. 1D) the latter two sequences are replaced by an eTOCSY-eINEPT sequence. In addition, the final $^{15}N \rightarrow {}^1H$ reverse INEPT transfer step has been replaced by an eINEPT sequence.

In the following, we describe the development of the coherences during the pulse sequence of the doubly enhanced 3D TOCSY-HSQC experiment (Fig. 1D) in terms of H^+, H^-, N^+, N^-, H_z and N_z (for conventions see Van de Ven, 1995). Starting with the excitation pulse,

$$\sigma_A = -H_x \tag{1}$$

is generated at point A (Fig. 1D), which evolves during t_1 into:

$$\begin{aligned}\sigma_B &= -H_x \cos(\omega_H t_1) + H_y \sin(\omega_H t_1) \\ &= -1/2\ \{H^+ e(i\omega_H t_1) + H^- e(-i\omega_H t_1)\}\end{aligned} \tag{2}$$

which after the 180°_x proton pulse and application of the gradient evolves into:

$$\begin{aligned}\sigma_C = -1/2\ &\{H^- e(i\omega_H t_1 - i\gamma_H g_1 \tau_1) \\ &+ H^- e(-i\omega_H t_1 + i\gamma_H g_1 \tau_1)\}\end{aligned} \tag{3}$$

at point C. Note that as compared to the non-enhanced version of the experiment (Fig. 1A) an additional delay period 2δ had to be included after the t_1 evolution period to incorporate the gradient. Subsequently, the eTOCSY-eINEPT transfer step gives at point D rise to:

$$\begin{aligned}\sigma_D^N = -1/2\ &\{-i\ 2H_z N^- e(i\omega_H t_1 - i\gamma_H g_1 \tau_1) \\ &+ i\ 2H_z N^+ e(-i\omega_H t_1 + i\gamma_H g_1 \tau_1)\} \quad (\phi_1 = x)\end{aligned} \tag{4}$$

when $\phi_1 = x$. This corresponds to the N-type signal. When $\phi_1 = -x$, the P-type signal is obtained:

$$\begin{aligned}\sigma_D^P = -1/2\ &\{+i\ 2H_z N^- e(i\omega_H t_1 - i\gamma_H g_1 \tau_1) \\ &- i\ 2H_z N^- e(-i\omega_H t_1 + i\gamma_H g_1 \tau_1)\} \quad (\phi_1 = -x)\end{aligned} \tag{5}$$

The subsequent ^{15}N evolution period t_2 is incorporated into a constant-time period of total fixed duration 2T. As a result, both the refocussing gradient for t_1 and the defocussing gradient for the second evolution period t_2 can be incorporated into the constant-time period without requiring extra delays. After the constant-time evolution period, the previously considered N- and P-type terms have at point E evolved into:

$$\begin{aligned}\sigma_E^N = &-1/2\ i\ 2H_z N^+ e(+i\omega_H t_1 - i\gamma_H g_1 \tau_1 \\ &- i\gamma_N g_2 \tau_2 + i\gamma_N g_3 \tau_3 - i\omega_N t_2) \\ &+ 1/2\ i\ 2H_z N^- e(-i\omega_H t_1 + i\gamma_H g_1 \tau_1 \\ &+ i\gamma_N g_2 \tau_2 - i\gamma_N g_3 \tau_3 + i\omega_N t_2) \\ &(\text{with } \phi_1 = x,\ \text{N-type})\end{aligned} \tag{6}$$

and

$$\begin{aligned}\sigma_E^P = &+1/2\ i\ 2H_z N^- e(+i\omega_H t_1 - i\gamma_H g_1 \tau_1 \\ &+ i\gamma_N g_2 \tau_2 - i\gamma_N g_3 \tau_3 + i\omega_N t_2) \\ &- 1/2\ i\ 2H_z N^+ e(-i\omega_H t_1 + i\gamma_H g_1 \tau_1 \\ &- i\gamma_N g_2 \tau_2 + i\gamma_N g_3 \tau_3 - i\omega_N t_2) \\ &(\text{with } \phi_1 = -x,\ \text{P-type})\end{aligned} \tag{7}$$

The subsequent reverse eINEPT period, which includes a refocussing gradient, links the evolution period t_2 with the acquisition period t_3. The separate P- and N-type terms, σ_E^P and σ_E^N, each give rise to both a P-type as well as an N-type term in this step, depending on the settings of ϕ_4. Finally, four possible terms arise at point F in the 3D doubly enhanced TOCSY-HSQC sequence:

$$\begin{aligned}\sigma_F^{NN} = &-1/2\ i\ H^+ e(+i\omega_H t_1 - i\gamma_H g_1 \tau_1 \\ &- i\gamma_N g_2 \tau_2 + i\gamma_N g_3 \tau_3 + i\gamma_H g_4 \tau_4 - i\omega_N t_2) \\ &+ 1/2\ i\ H^- e(-i\omega_H t_1 + i\gamma_H g_1 \tau_1 + i\gamma_N g_2 \tau_2 \\ &- i\gamma_N g_3 \tau_3 - i\gamma_H g_4 \tau_4 + i\omega_N t_2) \\ &(\text{with } \phi_1 = x,\ \text{N-type};\ \phi_4 = y,\ \text{N-type})\end{aligned} \tag{8}$$

$$\begin{aligned}\sigma_F^{NP} = &+1/2\ i\ H^- e(+i\omega_H t_1 - i\gamma_H g_1 \tau_1 \\ &- i\gamma_N g_2 \tau_2 + i\gamma_N g_3 \tau_3 - i\gamma_H g_4 \tau_4 - i\omega_N t_2) \\ &- 1/2\ i\ H^+ e(-i\omega_H t_1 + i\gamma_H g_1 \tau_1 + i\gamma_N g_2 \tau_2 \\ &- i\gamma_N g_3 \tau_3 + i\gamma_H g_4 \tau_4 + i\omega_N t_2 \\ &(\text{with } \phi_1 = x,\ \text{N-type};\ \phi_4 = -y,\ \text{P-type})\end{aligned} \tag{9}$$

$$\begin{aligned}\sigma_F^{PN} = &+1/2\ i\ H^- e(+i\omega_H t_1 - i\gamma_H g_1 \tau_1 \\ &+ i\gamma_N g_2 \tau_2 - i\gamma_N g_3 \tau_3 - i\gamma_H g_4 \tau_4 + i\omega_N t_2) \\ &- 1/2\ i\ H^+ e(-i\omega_H t_1 + i\gamma_H g_1 \tau_1 - i\gamma_N g_2 \tau_2 \\ &+ i\gamma_N g_3 \tau_3 + i\gamma_H g_4 \tau_4 - i\omega_N t_2) \\ &(\text{with } \phi_1 = -x,\ \text{P-type};\ \phi_4 = y,\ \text{N-type})\end{aligned} \tag{10}$$

$$\begin{aligned}\sigma_F^{PP} = &-1/2\ i\ H^+ e(+i\omega_H t_1 - i\gamma_H g_1 \tau_1 \\ &+ i\gamma_N g_2 \tau_2 - i\gamma_N g_3 \tau_3 + i\gamma_H g_4 \tau_4 + i\omega_N t_2) \\ &+ 1/2\ i\ H^- e(-i\omega_H t_1 + i\gamma_H g_1 \tau_1 - i\gamma_N g_2 \tau_2 \\ &+ i\gamma_N g_3 \tau_3 - i\gamma_H g_4 \tau_4 - i\omega_N t_2) \\ &(\text{with } \phi_1 = -x,\ \text{P-type};\ \phi_4 = -y,\ \text{P-type})\end{aligned} \tag{11}$$

Only the H^- terms will lead to detectable signal. Amplitude-modulated detectable H^- coherences can be obtained via proper linear combinations of the σ_F terms:

$$\sigma_F^{NN} + \sigma_F^{NP} + \sigma_F^{PN} + \sigma_F^{PP} = 2i\ H^- \cos(\omega_H t_1) \cos(\omega_N t_2) \tag{12a}$$

$$\sigma_F^{NN} - \sigma_F^{NP} + \sigma_F^{PN} - \sigma_F^{PP} = -2\ H^- \cos(\omega_H t_1) \sin(\omega_N t_2) \tag{12b}$$

$$\sigma_F^{NN} - \sigma_F^{NP} - \sigma_F^{PN} + \sigma_F^{PP} = 2\ H^- \sin(\omega_H t_1) \cos(\omega_N t_2) \tag{12c}$$

$$\sigma_F^{NN} + \sigma_F^{NP} - \sigma_F^{PN} - \sigma_F^{PP} = 2i\ H^- \sin(\omega_H t_1) \sin(\omega_N t_2) \tag{12d}$$

The signal amplitude is four times as large as that obtained for the conventional unenhanced sequence. The latter sequence namely, with the phases of the pulses as shown in Fig. 1A, gives rise to the detectable signals:

$$\sigma_{det} = 1/2\ H^- \cos(\omega_H t_1) \cos(\omega_N t_2) \tag{13a}$$

$$\sigma_{det} = 1/2\ H^- \cos(\omega_H t_1) \sin(\omega_N t_2) \tag{13b}$$

$$\sigma_{det} = 1/2\ H^- \sin(\omega_H t_1) \cos(\omega_N t_2) \tag{13c}$$

$$\sigma_{det} = 1/2\ H^- \sin(\omega_H t_1) \sin(\omega_N t_2) \tag{13d}$$

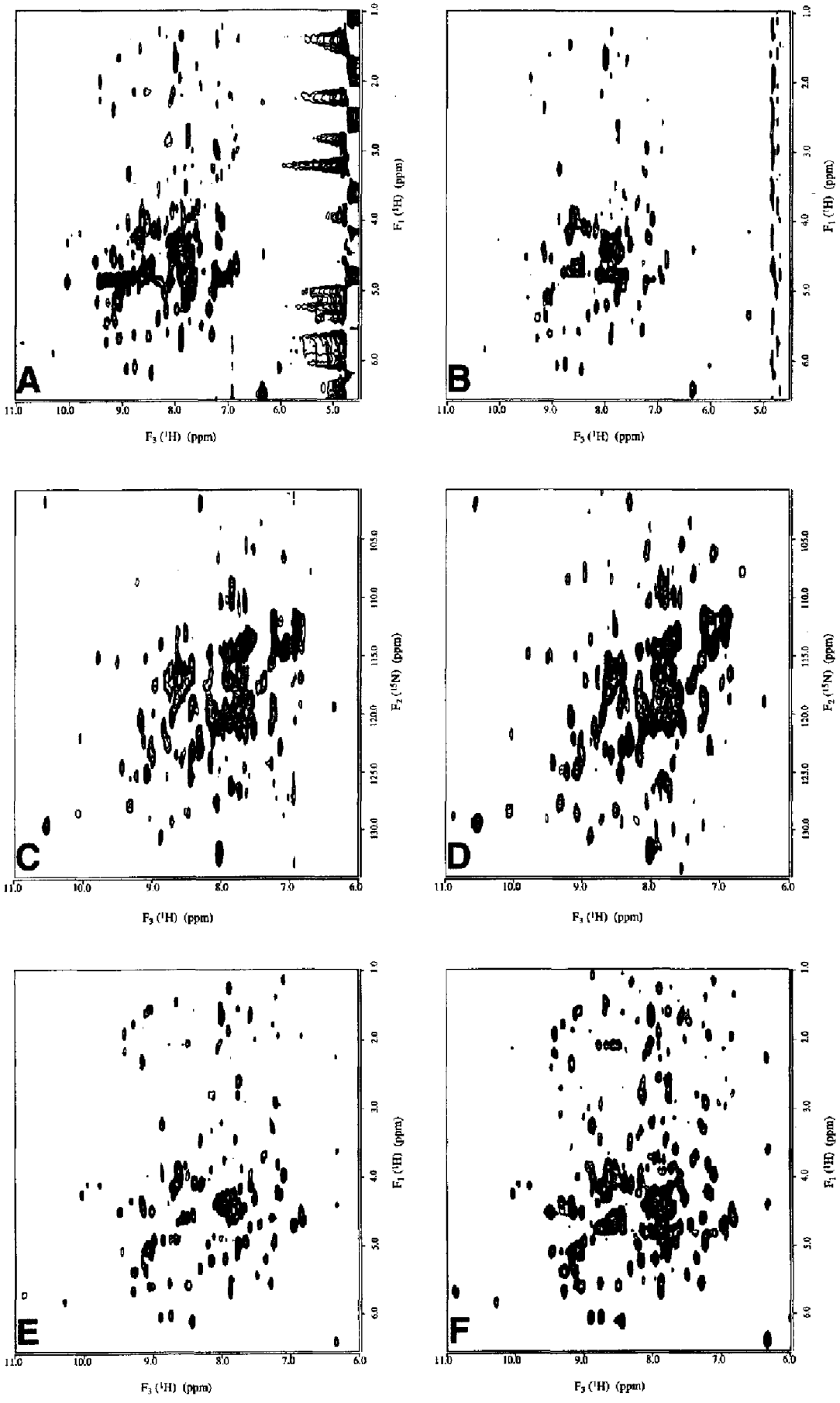
A
B
C
D
E
F
F3 (1H) (ppm)
F1 (1H) (ppm)
F2 (15N) (ppm)

It is important to realize that per free induction decay the same signal amplitudes are obtained in the conventional unenhanced and in the doubly enhanced versions of the 3D experiment, compare Eqs. 8–11 with Eqs. 13a–d. In case of the conventional sequence of Fig. 1A, both the cos- and sine-modulated signals have to be measured to obtain sign discrimination in F1 and F2 (Keeler and Neuhaus, 1985). Note that Eqs. 12a and 12d are 90° out of phase with respect to the corresponding terms obtained using the conventional sequence of Fig. 1A, as follows from the imaginary number i. Their correct phases are obtained by interchanging the imaginary and real parts of their FIDs and negating the imaginary parts of the resulting FIDs. Subsequent three-dimensional Fourier transformation of the amplitude-modulated H^- coherences leads to pure absorption-mode cross peaks with sign discrimination in F1 and F2.

The difference between the conventional experiment and the experiment employing gradients for coherence pathway selection is that the separately measured N- and P-type signals are added or subtracted for the latter experiment (Eqs. 12a–d). This procedure leads to an averaging of the noise by a factor of $4^{1/2}$. Hence, whereas the signal increases by a factor of 4 in the gradient-selected experiment, the ultimate signal-to-noise ratio increases only by a factor of 2 (i.e., 4 divided by $4^{1/2}$) as compared to the conventional experiment. This corresponds to a signal-to-noise improvement by a factor of 2.

To select a specific coherence pathway, the corresponding net phase resulting from the gradients incorporated into the pulse sequence has to be zero (see Eqs. 8–11):

$$\text{NN: } +i\gamma_H\, s1|g_1|\tau_1 + i\gamma_N\, s2|g_2|\tau_2 - i\gamma_N\, s3|g_3|\tau_3 - i\gamma_H\, s4|g_4|\tau_4 = 0 \quad (\phi_1 = x,\ \phi_4 = y) \tag{14a}$$

$$\text{NP: } -i\gamma_H\, s1|g_1|\tau_1 - i\gamma_N\, s2|g_2|\tau_2 + i\gamma_N\, s3|g_3|\tau_3 - i\gamma_H\, s4|g_4|\tau_4 = 0 \quad (\phi_1 = x,\ \phi_4 = -y) \tag{14b}$$

$$\text{PN: } -i\gamma_H\, s1|g_1|\tau_1 + i\gamma_N\, s2|g_2|\tau_2 - i\gamma_N\, s3|g_3|\tau_3 - i\gamma_H\, s4|g_4|\tau_4 = 0 \quad (\phi_1 = -x,\ \phi_4 = y) \tag{14c}$$

$$\text{PP: } +i\gamma_H\, s1|g_1|\tau_1 - i\gamma_N\, s2|g_2|\tau_2 + i\gamma_N\, s3|g_3|\tau_3 - i\gamma_H\, s4|g_4|\tau_4 = 0 \quad (\phi_1 = -x,\ \phi_4 = -y) \tag{14d}$$

in which s1 to s4 represent the sign of gradients g_1 to g_4, respectively. Since four gradients are used, a certain element of freedom remains to achieve the desired coherence pathway selection. Both the number of gradients used as well as their length or amplitude may be altered. Firstly, it can be concluded that only one gradient during the constant-time period would suffice for coherence pathway selection in both the t_1 and the t_2 evolution period. However, we instead have chosen to use two gradients during the constant-time evolution period. This has the advantage that one can achieve coherence pathway selection independently for each of the two transfer steps and thereby test the quality of each individual selection step. Secondly, we have decided to keep both the gradient amplitudes and lengths constant: $|g_2|\tau_2 = +(\gamma_H/\gamma_N)\ |g_1|\tau_1$ and $|g_3|\tau_3 = +(\gamma_H/\gamma_N)\ |g_4|\tau_4$. Consequently, coherence pathway selection of the four different routes can be achieved by simply permuting the signs of the first and last gradients:

$$\text{NN: } s(-,+,+,-) \tag{15a}$$

$$\text{NP: } s(-,+,+,+) \tag{15b}$$

$$\text{PN: } s(+,+,+,-) \tag{15c}$$

$$\text{PP: } s(+,+,+,+) \tag{15d}$$

To keep the delays δ and ε in the pulse sequence as short as possible, we decided to choose a duration of 0.125 ms for the first gradient with a recovery time of 0.125 ms, so that δ = 2 * 0.125 ms. Similarly, the final gradient lasted 0.25 ms with a recovery time of 0.25 ms,

←

Fig. 2. Two-dimensional initial planes ($t_1 = 0$ or $t_2 = 0$) from 3D TOCSY-HSQC experiments obtained by using the sequences in Fig. 1 for either a uniformly 5 mM ^{13}C-/^{15}N-labeled (A, B, C and D) or a 3 mM uniformly ^{15}N-labeled (E and F) flavodoxin sample. The planes demonstrate the effect of several factors on the signal intensities. Firstly, planes A and B demonstrate the combined effect of exclusion of presaturation and inclusion of a Gaussian flip-back pulse on the TOCSY-HSQC experiment. (A) ^1H-^1H plane recorded with the doubly enhanced pulse sequence 1E ($t_2 = 0$); no presaturation is used and a Gaussian flip-back pulse is included, which positions the water magnetization along the +z-axis prior to acquisition. (B) ^1H-^1H plane recorded with the doubly enhanced pulse sequence 1D ($t_2 = 0$); the solvent is presaturated and the Gaussian flip-back pulse results in dephasing of any residual water (see text); for comparison, the contour levels are set to the values used in (A). Secondly, planes C and D demonstrate the effect of enhancement of the reverse INEPT part on the TOCSY-HSQC experiment. (C) ^{15}N-^1H plane recorded with the standard non-enhanced sequence 1A ($t_1 = 0$) with presaturation. (D) ^{15}N-^1H plane recorded with the singly enhanced sequence 1B ($t_1 = 0$) with solvent presaturation and the phase of the Gaussian flip-back pulse set to x, so that net dephasing of the transverse water magnetization is achieved. For comparison, the contour levels are set to the values used in C. Thirdly, planes E and F demonstrate the effect of enhancement of the TOCSY-INEPT part on the TOCSY-HSQC experiment. (E) ^1H-^1H plane recorded with the singly enhanced sequence 1B ($t_2 = 0$) with presaturation. (F) ^1H-^1H plane recorded with the doubly enhanced sequence 1D ($t_2 = 0$) with presaturation; for comparison, the contour levels are set to the values used in E. All spectra were recorded with the following settings: spectral widths of 9615 Hz in the proton dimensions, and 2057 Hz in the ^{15}N dimension, 512 and 64 complex points in the ^1H acquisition and ^1H indirect dimension, respectively, and 32 complex points in the ^{15}N dimension; 32 FIDs were accumulated per increment. All acquired data were processed identically. Prior to Fourier transformation, the FIDs were multiplied by a quadratic cosine filter in both dimensions and zero-filled. All spectra were acquired on a Bruker AMX2 600 spectrometer equipped with a triple resonance probehead with a doubly tuned {^1H,^{13}C} inner coil and a broadband outer coil and a self-shielded z-gradient coil.

so that $\varepsilon = 2 * 0.25$ ms. The second and third gradient were both chosen to last 0.5 ms and each was associated with a 0.5 ms recovery time. Consequently, the ratio of the amplitudes of gradients 1, 2, 3 and 4 is now fixed. We used gradient strengths of 16, 40, 80 and 16 (with 100 corresponding to 60 G/cm), for gradients 1, 2, 3 and 4, respectively.

The second and third gradient deliberately have the same sign, as this results in additive defocussing of unwanted residual ^1H coherences corresponding to protons not bound to ^{15}N atoms. As the change of gradient signs necessary for coherence pathway selection takes place on the relatively weak and short first and last gradient in the pulse sequence, the resulting variation in total defocussing of such unwanted coherences is limited.

The doubly enhanced 3D TOCSY-HSQC pulse sequence contains extra delay periods as compared to the standard pulse sequence, but in contrast to the standard sequence, it does not need the two trim pulses around the DIPSI3$_x$ sequence. Consequently, the net lengthening of the pulse sequence as compared to the standard sequence is: $2\delta + 2\tau + 2\tau + 2\varepsilon - 2\,\text{trim} = 0.5\text{ ms} + 4.5\text{ ms} + 4.5\text{ ms} + 1.0\text{ ms} - 5\text{ ms} = 5.5$ ms. When we neglect the effect of rf inhomogeneity, the doubly enhanced pulse sequence is only expected to perform poorer in terms of sensitivity as compared to the standard sequence when $2 * \exp -5.5\text{ ms}/T2 < 1$. This is the case when $T2 > 8$ ms, which roughly corresponds to proteins with a molecular weight well over 20 kDa.

Much attention has recently been given to the effect of water suppression on the signal intensity of relatively rapidly exchanging NH protons (Grzesiek and Bax, 1993; Jahnke and Kessler, 1994; Stonehouse et al., 1995). The standard technique of water suppression has been presaturation of the water magnetization during the relaxation delay. As a result of the exchange of water protons with rapidly exchanging NH protons, the magnetization of NH protons also becomes partly saturated, which leads to a loss of NH signal intensity (see e.g. Grzesiek and Bax, 1993). When instead of presaturation B_0 field gradients are used to defocus the residual water signal, the possibility of incomplete recovery of water magnetization during the relaxation delay period exists. This also leads to a loss of signal intensity (Grzesiek and Bax, 1993; Jahnke and Kessler, 1994; Stonehouse et al., 1995). Hence, both methods should be avoided whenever possible. Instead, the water magnetization needs to be positioned along the +z-axis at the start of the acquisition, so that exchange of NH protons with water protons does not lead to signal loss.

In the singly enhanced 3D TOCSY-HSQC sequence (Fig. 1B), an optimal positioning of the water magnetization can be achieved by simply including a Gaussian water flip-back pulse with phase y prior to the first gradient. The water magnetization then lies along the +z-axis when the first gradient is applied and since the eINEPT sequence positions it ultimately again along the +z-axis just before the second gradient is applied, no defocussing of the water magnetization takes place at all. On the other hand, in both the gradient-selected singly enhanced pulse sequence of Fig. 1C and the doubly enhanced pulse sequence of Fig. 1D the water magnetization is defocussed by the first gradient. The pulse phases are chosen in such a way that as a consequence a fan of water magnetization vectors lies in the XY-plane just prior to the Gaussian flip-back pulse. This pulse, which has phase −x, rotates this fan into the XZ-plane. The water magnetization is thus only partially positioned along the +z-axis. The remaining transverse water component is subsequently defocussed by the second, third and fourth gradient. This approach is expected to result in a good solvent suppression, but it is not optimal for detecting rapidly exchanging amide protons because only part of the water magnetization vectors lies along the +z-axis prior to acquisition.

Thanks to the flexibility in choosing both the amplitudes and the positions of the second and third gradients in pulse sequences 1C and 1D, these sequences can easily be modified in such a way that the water magnetization is no longer defocussed and is positioned along the +z-axis at the start of acquisition. Such an optimized doubly enhanced pulse sequence is shown in Fig. 1E. The second gradient is now placed directly in front of the Gaussian water flip-back pulse and is used to refocus the water coherence, which was defocussed by the first gradient. The Gaussian water flip-back pulse subsequently rotates the refocussed water coherence to the +z-axis. The third gradient can then be used to select the coherences of interest by properly adjusting its amplitude. To select a specific coherence pathway, the net phase resulting from the gradients incorporated into the pulse sequence has to be zero. We can use the former scheme (Eq. 14) with the new prerequisite $|g_2|\tau_2 = |g_1|\tau_1$ with $s1 = -s2$ to refocus the water coherence. The amplitudes of the first, second and last gradient can be set to fixed values, which then determine the amplitude of the third gradient: we choose s3 positive and $|g_3|\tau_3 = +(\gamma_H/\gamma_N)\,|g_1|\tau_1 + (\gamma_H/\gamma_N)\,|g_4|\tau_4 +/- |g_1|\tau_1$. Coherence pathway selection can now be obtained by permuting the signs of the first, second and last gradients as follows:

$$\text{NN: } s(+,-,+,-) \tag{16a}$$

$$\text{NP: } s(+,-,+,+) \tag{16b}$$

$$\text{PN: } s(-,+,+,-) \tag{16c}$$

$$\text{PP: } s(-,+,+,+) \tag{16d}$$

Note that for the NN and NP pathways $|g_3|\tau_3 = +(\gamma_H/\gamma_N) \times |g_1|\tau_1 + (\gamma_H/\gamma_N)\,|g_4|\tau_4 - |g_1|\tau_1$ while for the PN and PP pathways $|g_3|\tau_3 = +(\gamma_H/\gamma_N)\,|g_1|\tau_1 + (\gamma_H/\gamma_N)\,|g_4|\tau_4 + |g_1|\tau_1$.

Results and Discussion

With respect to the sensitivity of a 3D TOCSY-HSQC experiment, two main aspects are expected to be of importance: (i) the water suppression method, and (ii) the enhancement resulting from the introduction of the COSCTs. To investigate how these aspects affect the sensitivity, we recorded a set of 2D planes corresponding to the pulse sequences shown in Fig. 1. The ratios of the corresponding cross-peak amplitudes of such 2D spectra give the relative changes in the signal intensities and thereby allow to establish the relative importance of the aforementioned aspects.

Firstly, we consider the effect of the water suppression method. Figure 2A shows the ^{1}H-^{1}H plane recorded using the doubly enhanced sequence 1E without presaturation (but with flip-back pulse). A similar plane, recorded using the doubly enhanced pulse sequence 1D but with presaturation, is shown in Fig. 2B. The comparison of Fig. 2A with Fig. 2B directly demonstrates the drastic increase in signal intensity, resulting from the combined effect of (i) exclusion of presaturation and (ii) inclusion of the Gaussian flip-back pulse. To estimate solely the effect of presaturation, we recorded a ^{1}H-^{1}H spectrum without presaturation (not shown), using the doubly enhanced pulse sequence 1E from which the Gaussian flip-back pulse has been removed, and compared it to the presaturated spectrum shown in Fig. 2B (the Gaussian flip-back pulse in the latter sequence causes dephasing of the water magnetization for any setting of its pulse phase; see previous section). The ratios of the corresponding cross-peak amplitudes are shown in the histogram in Fig. 3A. On avoiding presaturation, an average improvement of a factor of 1.47 is found for the cross-peak amplitudes in the ^{1}H-^{1}H planes. Similarly, we found an average cross-peak amplitude improvement of 1.38 for the ^{15}N-^{1}H planes (not shown) using the singly enhanced pulse sequence 1B either with or without presaturation (note that both spectra were recorded with the phase of the Gaussian pulse set to −x, so that no flip-back of the water magnetization occurred). To estimate solely the effect of the water flip-back pulse itself, a comparison was made of the ^{1}H-^{1}H planes (not shown) recorded using the doubly enhanced sequence 1E, either with or without Gaussian flip-back pulse (in both cases water presaturation was avoided). The relative peak amplitudes of the cross peaks in the two spectra are shown in the histogram in Fig. 3B. Only a slight improvement in sensitivity of on average a factor of 1.07 results from the inclusion of such a water flip-back pulse. We can thus conclude that the omission of presaturation significantly increases the sensitivity, whereas the inclusion of a Gaussian flip-back pulse only results in a slight improvement. The large effect of the inclusion of presaturation is a result of transfer of saturated magnetization from water protons to NH protons. This exchange takes place during the whole relaxation delay period of 1 s. The effect of inclusion of a Gaussian flip-back pulse without the use of presaturation is small. The reason for this is that without a flip-back pulse the defocussed water magnetization recovers relatively quickly due to radiation damping (in about 300 to 500 ms). Consequently, the remaining time in the relaxation delay suffices for the NH magnetization to relax back to the +z-axis.

Secondly, to investigate the effect of the reverse eINEPT part, we compare the ^{15}N-^{1}H plane recorded using the singly enhanced sequence 1B with the one recorded employing the standard non-enhanced sequence 1A (using the ^{13}C-/^{15}N-enriched flavodoxin sample). The ^{15}N-^{1}H planes are shown in Figs. 2C and 2D, respectively. To correctly estimate the effect of single enhancement, both ^{15}N-^{1}H planes were recorded with presaturation and with a Gaussian flip-back pulse included, which has a phase such that the water coherence is not returned to the +z-axis. In Fig. 3C the histogram of the ratios of the cross-peak amplitudes of the two spectra demonstrates the effect of enhancement of the reverse INEPT part on the TOCSY-HSQC experiment. As can be seen, the peak amplitudes increase significantly on using the singly enhanced pulse sequence. The average enhancement factor is 1.55. This factor is lower than the theoretically expected maximum of two. Note that in order to establish the improvement in signal-to-noise ratio this factor of 1.55 should be divided by $2^{1/2}$, since the noise in the singly enhanced spectrum is a factor of $2^{1/2}$ higher than in the standard spectrum, as discussed before.

Thirdly, to investigate the effect of enhancement of the TOCSY-INEPT part on the TOCSY-HSQC experiment we compared ^{1}H-^{1}H planes recorded using the doubly enhanced sequence 1D and the singly enhanced sequence 1B, respectively (with the ^{15}N-enriched flavodoxin sample). Both spectra were recorded with presaturation to ensure a correct comparison. The obtained ^{1}H-^{1}H spectra are shown in Figs. 2F and 2E, respectively. The ratios of the cross-peak amplitudes of the doubly enhanced spectrum and of the singly enhanced spectrum are shown in Fig. 3D. Again, a significant increase in signal intensity of on average 1.78 is found.

Thus, replacing the TOCSY-INEPT sequence and the reverse INEPT sequence by their enhanced counterparts which include gradients leads to signal enhancements of 1.78 and 1.55, respectively. At first sight it seems not surprising that both values are lower than the theoretically expected factor of 2, since the enhanced pulse sequences are slightly longer and contain more pulses. The lower value of 1.55 obtained for the ^{13}C-/^{15}N-enriched flavodoxin sample as compared to the value of 1.78 obtained for the ^{15}N-enriched sample is consistent with the idea that smaller T2 values (in the doubly enriched sample) will lead to an increased signal loss.

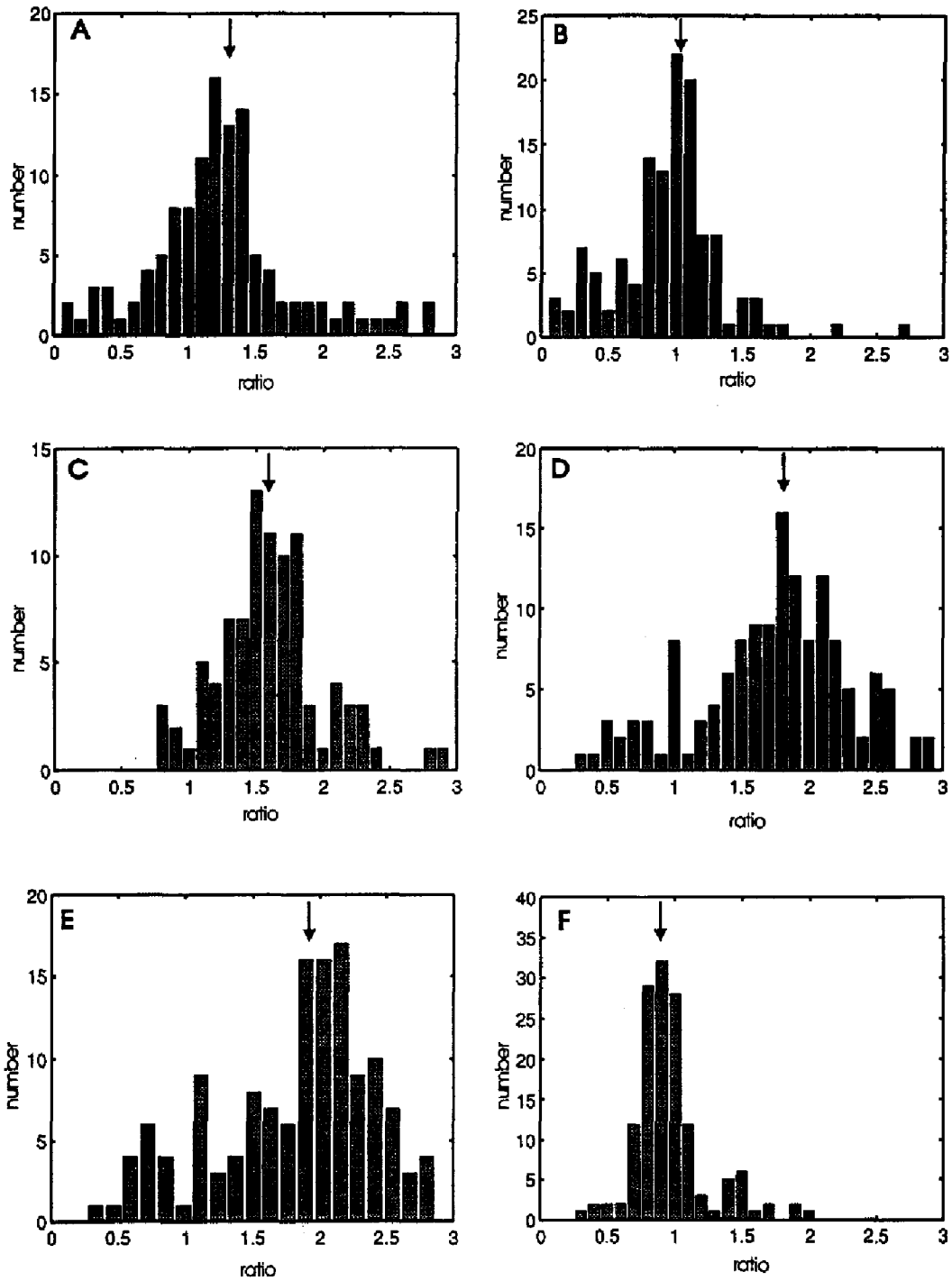

Fig. 3. Histograms of the relative cross-peak amplitudes (I over II), demonstrating the effects of several factors on the signal enhancement of the TOCSY-HSQC experiment. The height of each bar represents the number of residues with the indicated relative cross-peak amplitude. The arrows indicate the average enhancements obtained. (A) The effect of presaturation: sequence 1E without presaturation and without flip-back pulse (I) is compared to sequence 1D with presaturation (II); both sequences were used to acquire ^{1}H-^{1}H planes. (B) The effect of introducing a Gaussian water flip-back pulse: a comparison of sequence 1E with (I) and without (II) Gaussian flip-back pulse. ^{1}H-^{1}H planes were acquired. Both spectra were recorded without presaturation. (C) The effect of enhancement of the reverse INEPT part: the singly enhanced sequence 1B (I) is compared with the standard non-enhanced sequence 1A (II); ^{15}N-^{1}H planes were acquired. Both spectra were recorded with presaturation. (D) The effect of enhancement of the TOCSY-INEPT part: the doubly enhanced sequence 1D (I) is compared with the singly enhanced sequence 1B (II); ^{1}H-^{1}H planes were acquired. Both planes were recorded with presaturation. (E) The effect of enhancement of the TOCSY-INEPT part under exclusion of potential gradient effects (see text): the doubly enhanced sequence 1D (I) is compared with the singly enhanced sequence 1C (II); ^{1}H-^{1}H planes were acquired. Both planes were recorded with presaturation. (F) The effect of the mere inclusion of gradients for coherence pathway selection: the singly enhanced sequence 1C (I) is compared with the singly enhanced sequence 1B (II); ^{1}H-^{1}H planes were acquired. Both planes were recorded with presaturation. For (A), (B) and (C) a uniformly ^{13}C-/^{15}N-enriched flavodoxin sample was used, and for (D), (E) and (F) a uniformly ^{15}N-enriched flavodoxin sample.

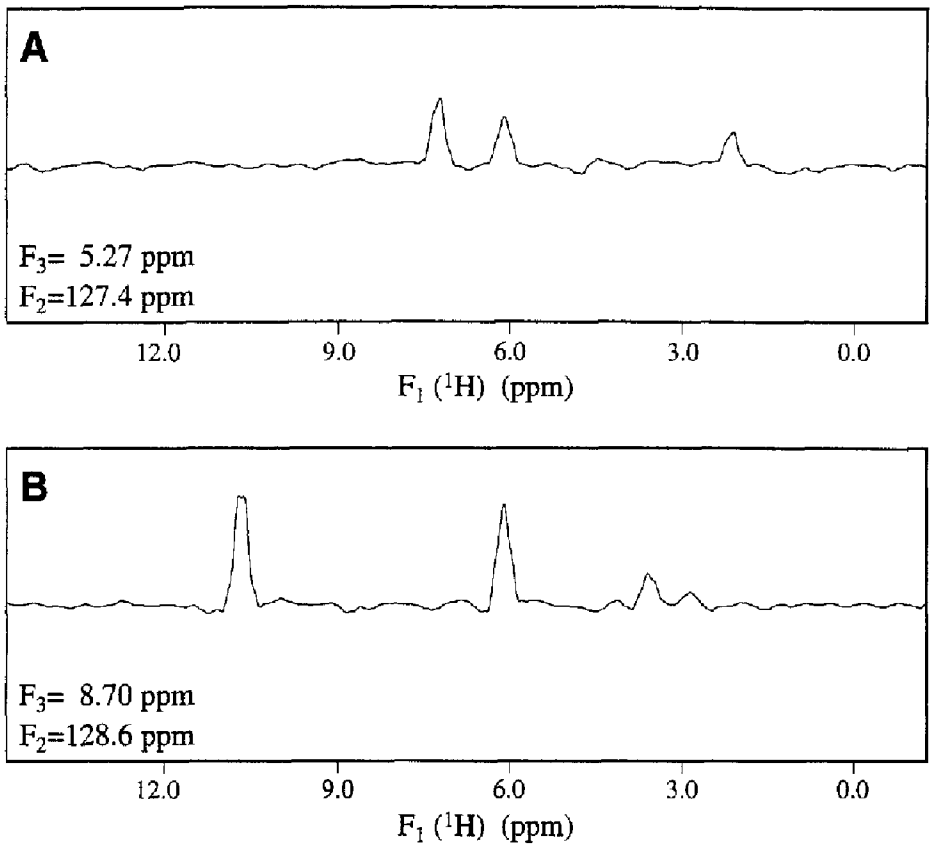

Fig. 4. One-dimensional slices through (A) F2 = 127.4 ppm and F3 = 5.27 ppm and (B) F2 = 128.6 ppm and F3 = 8.70 ppm of the 3D doubly enhanced TOCSY-HSQC spectrum obtained with sequence 1D. A 3 mM uniformly ^{15}N-labeled flavodoxin sample was used.

To exclude the potential effect of the introduction of gradients on the enhancement obtained by replacing the TOCSY-INEPT part by eTOCSY-eINEPT, we recorded a ^{1}H-^{1}H plane with pulse sequence 1C and compared its cross-peak amplitudes with those of the ^{1}H-^{1}H spectrum recorded with sequence 1D (Fig. 2F, using the ^{15}N-enriched flavodoxin sample). Since the pulse sequences only differ by the replacement of the TOCSY-INEPT sequence (sequence 1C) by an eTOCSY-eINEPT sequence (sequence 1D), a theoretical signal enhancement of a factor of 2 is expected. In Fig. 3E the ratios of the cross-peak amplitudes are shown. Indeed, now an enhancement factor of nearly 2 is observed for the majority of the NH protons (on average a factor of 1.87). This demonstrates that the loss in signal intensity due to the presence of additional pulses and to an increase of the total duration of the pulse sequence is rather limited for the ^{15}N-enriched sample of this relatively large protein. It also suggests that the mere inclusion of gradients for coherence pathway selection leads to a reduction in signal intensity. That the latter is true follows from Fig. 3F, in which the histogram is shown of the ratios of the cross-peak amplitudes obtained with pulse sequence 1C to those obtained with pulse sequence 1B. Indeed, a slight but significant decrease of on average 0.92 is observed. Thus, the mere inclusion of gradients for coherence pathway selection leads to a signal loss of about 8%. The previously discussed single enhancement factors of 1.55 for the eTOCSY-eINEPT part and of 1.78 for the reverse eINEPT part for the ^{13}C-/^{15}N-enriched and for the ^{15}N-enriched flavodoxin samples, respectively, are lower than the theoretically expected maximum of 2. We now know that these lower values are not only due to the lengthening of the pulse sequences, but that they are also partly caused by the inclusion of gradients.

The overall gain in signal intensity on using the doubly enhanced TOCSY-HSQC sequence (1E) as compared to the standard sequence (1A) can therefore be estimated to be 4.98 (= 1.78 * 1.78 * 1.47 * 1.07) and 3.78 (= 1.55 * 1.55 * 1.47 * 1.07) for the ^{15}N- and ^{13}C-/^{15}N-enriched flavodoxin samples, respectively. To obtain the corresponding signal-to-noise improvements, the gain should be divided by 2. This gives overall signal-to-noise enhancements of 2.49 and 1.89, respectively.

Finally, a high-quality 3D spectrum is obtained, as can be inferred from the two slices shown in Figs. 4A and 4B.

Conclusions

We have presented pulse sequences for singly and doubly enhanced 3D TOCSY-HSQC experiments and

demonstrated their application on both ^{13}C-/^{15}N- and ^{15}N-enriched samples of the relatively large (179 amino acid residues) protein flavodoxin. Good artifact and solvent suppression is observed. The singly and doubly enhanced 3D TOCSY-HSQC pulse sequences can be set up in such a way that (i) presaturation is avoided and (ii) the water magnetization vector is not defocussed by the gradients and lies along the +z-axis just prior to the start of acquisition. This provides optimal sensitivity for rapidly exchanging NH protons. The net overall improvement in signal-to-noise ratio with respect to the standard sequence is 2.49 for the doubly enhanced version of the pulse sequence using a ^{15}N-enriched flavodoxin sample. A significant part of this total improvement, namely a factor of 1.47, stems from the elimination of water presaturation. Hence, the net overall gain in signal-to-noise ratio resulting from the double enhancement procedure as compared to the standard sequence is 1.58, when excluding the effect of water presaturation and of the flip-back pulse. This value should be compared to the theoretical maximum enhancement of 2. We found that the lower value of 1.58 is partly due to the incorporation of gradients, since introduction of the enhanced coherence transfer sequence alone does give an enhancement close to the theoretically expected value.

Acknowledgements

The research of Carlo P.M. van Mierlo has been made possible by a fellowship of the Royal Netherlands Academy of Arts and Sciences.

References

Bax, A. and Pochapsky, S. (1992) *J. Magn. Reson.*, **99**, 638–643.
Cavanagh, J. and Rance, M. (1990) *J. Magn. Reson.*, **88**, 72–85.
Grzesiek, S. and Bax, A. (1993) *J. Am. Chem. Soc.*, **115**, 12953–12954.
Jahnke, W. and Kessler, H. (1994) *J. Biomol. NMR*, **4**, 735–740.
Kay, L.E. (1995) *Curr. Opin. Struct. Biol.*, **5**, 674–681.
Kay, L.E., Keifer, P. and Saarinen, T. (1992) *J. Am. Chem. Soc.*, **114**, 10663–10665.
Keeler, J. and Neuhaus, D. (1985) *J. Magn. Reson.*, **63**, 454–472.
Keeler, J., Clowes, R.T., Davis, A. and Laue, E.D. (1994) *Methods Enzymol.*, **239**, 145–207.
Kontaxis, G., Stonehouse, J., Laue, E.D. and Keeler, J. (1994) *J. Magn. Reson.*, **A111**, 70–76.
Krishnamurthy, V.V. (1995) *J. Magn. Reson.*, **B106**, 170–177.
Marion, D., Ikura, M., Tschudin, R. and Bax, A. (1989) *J. Magn. Reson.*, **85**, 393–399.
Palmer III, A.G., Cavanagh, J., Wright, P.E. and Rance, M. (1991) *J. Magn. Reson.*, **93**, 151–170.
Sattler, M., Schwendinger, M., Schleucher, J. and Griesinger, C. (1995a) *J. Biomol. NMR*, **6**, 11–22.
Sattler, M., Schmidt, P., Schleucher, J., Schledetzky, O., Glaser, S.J. and Griesinger, C. (1995b) *J. Magn. Reson.*, **B108**, 235–242.
Schleucher, J., Schwendinger, M., Sattler, M., Schmidt, P., Schledetzky, O., Glaser, S.J., Sörensen, O.W. and Griesinger, C. (1994) *J. Biomol. NMR*, **4**, 301–306.
Shaka, A.J., Barker, P.B. and Freeman, R. (1985) *J. Magn. Reson.*, **64**, 547–558.
Shaka, A.J., Lee, C.J. and Pines, A. (1988) *J. Magn. Reson.*, **77**, 274–293.
Stonehouse, J., Shaw, G.L., Keeler, J. and Laue, E.D. (1994) *J. Magn. Reson.*, **A107**, 178–184.
Stonehouse, J., Clowes, T.C., Shaw, G.L., Keeler, J. and Laue, E.D. (1995) *J. Biomol. NMR*, **5**, 226–232.
Van de Ven, F.J.M. (1995) *Multi-dimensional NMR in Liquids*, VCH Publishers, Cambridge, U.K., pp. 71–72.